A REGULATION OF TROPICAL CLIMATE BY RADIATIVE COOLING AS SIMULATED IN A CUMULUS ENSEMBLE MODEL

C.-H. Sui, K.-M. Lau, X. Li, and M.-D. Chou
Laboratory for Atmospheres, Goddard Space Flight Center, NASA

July 2000
To be submitted to J. of Climate

A REGULATION OF TROPICAL CLIMATE BY RADIATIVE COOLING AS SIMULATED IN A CUMULUS ENSEMBLE MODEL

C.-H. Sui, K.-M. Lau, X. Li, and M.-D. Chou
Laboratory for Atmospheres, Goddard Space Flight Center, NASA

April 2000

ABSTRACT

Responses of tropical atmosphere to low-boundary forcing are investigated in a 2-D cumulus ensemble model (CEM) with an imposed warm-pool and cold-pool SST contrast (δSST). The domain-mean vertical motion is constrained to produce heat sink and moisture source as in the observed tropical climate. In a series of experiments, the warm pool SST is specified at different values while the cold pool SST is specified at 26°C. The strength of the circulation increases with increasing δSST until δSST reaches 3.5 °C, and remains unchanged as δSST exceeds 3.5°C. The regulation of tropical convection by zonal SST gradient is constrained by the radiative cooling over the cold pool. For δSST < 3.5°C, an enhanced subsidence warming is balanced by a reduced condensation heating over the cold pool. For δSST > 3.5°C, the subsidence regime expands over the entire cold pool where no condensation heating exist so that a further enhanced subsidence warming can no longer be sustained.

The above regulation mechanism is also evident in the change of energy at the top of the atmosphere (TOA) that is dominated by cloud and water vapor greenhouse effect (c_{LW} and G_{clear}). The change in shortwave radiation at TOA is largely canceled between the warm pool and cold pool, likely due to the same imposed vertical motion in our experiments. For δSST<3.5°C, an increase of δSST is associated with a large increase in c_{LW} due to increased total clouds in response to enhanced SST-induced circulation. For δSST>3.5°C, clouds over the warm pool decrease with increasing SST, and the change in c_{LW} is much smaller. In both dSST regimes, the change in c_{LW} is larger than the change in G_{clear} which is slightly negative. However, in the case of uniform warming (δSST=0), ΔG_{clear} is positive, ~ 5 Wm^{-2} per degree change of SST.

1. INTRODUCITON

Interaction of cloud and water vapor with radiation and large-scale dynamics play a major role in the regulation of sea surface temperature and tropical climate. A better understanding and representation of these processes in climate models have been a major focus in climate research. Recently cumulus ensemble models (CEM) have been used for such a climate study because of the explicit treatment of convective-radiative processes in CEMs than in climate models. Among some of these studies, Held et al. (1993) studied the radiative-convective equilibrium in a CEM under different large-scale constraints. Sui et al. (1994) analyzed the tropical equilibrium water and heat budgets in a CEM. They showed a realistic model water cycle, and identified evaporation of clouds as important moisture source in the middle and upper troposphere, a process central to the cloud and water vapor feedback problem (e.g. Betts 1990, Sun and Lindzen 1993, Linden et al. 2000). Grabowski et al. (1996) performed a similar study using a different CEM. The equilibrium state of their model is different from that of Sui et al. (1994) despite similar experimental designs. The causes are discussed in Tao et al (1999) and Xu and Randall (1999).

CEMs have also been used to study climate feedback issues. Lau et el. (1993) applied the same CEM as used in Sui et al (1994) to study the convective-radiative equilibrium of the model to several perturbed climate conditions in the tropics. Their model response to a surface warming is consistent with those from general circulation models (GCM). Sui et al (1993) and Lau et al. (1994) applied the CEM results to explain observational analysis by Ramanathan and Collins (1991). They found that the change in cloud radiative forcing induced by local surface warming in the model is one order magnitude smaller than those induced by changes in large-scale circulation. They argued that both local processes and large-scale dynamics need to be

considered in studying cloud feedbacks. Tompkins and Craig (1998) used a three-dimensional CEM to study radiative convective equilibrium.

An obvious limitation of CEM studies by Sui et al (1993) and Lau et al (1993, 1994) in the study of cloud/water vapor responses to surface SST changes is the lack of large-scale feedback between the tropical convective regime and the surrounding subsidence regime. On important aspect of the large-scale feedbacks between the two regimes is the contribution of radiative cooling in the broad subsidence regime to the net water vapor feedback effect as emphasized by Lindzen (1990) in the global warming scenario. The clear-sky water vapor greenhouse effect is also discussed by Pierrehumbert (1995) who regards water vapor and convection over the tropical warm pool as furnace, and radiative cooling in the subsidence region as a fin. The radiator fin regulates tropical sea surface temperature and keeps the tropical climate from falling into a runaway greenhouse state.

In this study, we extend our previous modeling works by adding a subsidence climate regime to the ascending climate regime by an imposed SST distribution in the CEM. Our focus is to examine the perturbed climate in response to SST changes that induce not only local changes in the deep convective regime and the subsidence regime but also remote changes through interactions between the two regimes. The model and experiment designs are discussed in section 2. The equilibrium solution of a control experiment is discussed in section 3. The perturbed equilibrium solution due to increased basin-scale SST gradient is discussed in section 4. The relationship between water vapor and cloud radiative forcing and SST changes is discussed in section 5. The conclusion is summarized in section 6.

2. MODEL AND NUMERICAL EXPERIMENTS

The CEM used in this study is developed at Goddard Space Flight Center as described in Tao and Simpson (1993). The model consists of nonhydrostatic and anelastic set of equations for potential temperature, water vapor mixing ratio, winds, and five cloud species as expressed as θ, q_v, u, v, w, and q_{ci}, respectively. The 2-D version of the model used by Sui et al. (1994) with modified treatments of solar radiative and cloud microphysical processes is used here. The modified model is shown by Li et al. (1999) to produce better simulations in response to the imposed large-scale forcing as evaluated against TOGA COARE observations.

An important model design in the current study is to introduce a heat sink and moisture source as observed in the current tropical climate. This is achieved by imposing a time- and horizontal-independent vertical profile of upward motion in the model, as indicated by the following thermodynamic equations

$$\frac{\partial A}{\partial t} = -\nabla \bullet \bar{V}'A' - \frac{1}{\bar{\rho}}\frac{\partial}{\partial z}\bar{\rho}w'A' - \overline{w}\frac{\partial A'}{\partial z} - w'\frac{\partial \overline{A}}{\partial z} + S_A + D_A - \overline{w}\frac{\partial \overline{A}}{\partial z} \qquad (1)$$

where $A=(\theta, q_v)$, $A= \overline{A}+A'$, $\overline{A}$ denotes the domain mean variable, and domain mean zonal wind is assumed 0. The imposed upward motion gives rise to a moisture source and a heat sink (the last term in the above equation). The same profile of mean upward motion is imposed in all experiments. Other model equations consist of conservation equations for five cloud species and perturbation momentum equations. See Li et al. (1999) for more details.

Experiments are performed in an ocean domain of 5120 km along the equator with an idealized SST distributions of a warm pool about 1588 km wide in the center and a cold pool on both sides. Three experiments are performed with the warm pool SST specified at 28.5°C, 29.5°C, and 30.5°C respectively, and the cold pool SST at 26°C. These three experiments are

denoted as R, R1, and R2 as listed in Table 1. These three experiments are designed to study the effect of radiation-dynamic interaction in the cold pool on tropical climate (section 4). A fourth experiment, W, is performed by specifying the warm pool and cold pool SST at values of 1°C higher than the corresponding SSTs of Experiment R. This experiment together with other experiments are designed to examine the water vapor and cloud feedback mechanisms (section 5).

Table 1.

	Warm pool SST	Cold pool SST
R2	30.5	26
R1	29.5	26
R	28.5	26
W	29.5	27

Integration starts from an atmosphere at rest with zonally uniform temperature and moisture obtained from the observed mean values over the western Pacific. No cloud is present initially. All experiments are integrated for 50-70 days to reach equilibrium.

3. EQUILIBRIUM SOLUTION OF EXPERIMENT R1

Figure 1 shows the temporal evolution of vertically averaged temperature and moisture over the warm pool and cool pool, respectively, for the control experiment (R1). The model reaches an equilibrium state in about 15 days. The equilibrium solution is characterized by a moist state over the warm pool, a dry state over the cold pool, and almost the same mean temperature in the two regimes. The equilibrium state is a result of the "Walker" type circulation induced by SST gradient so air ascends over the warm pool and descends over the cold pool as revealed by the mean vertical motion over the two regimes for the period of Day 40 to Day 50 (Fig. 2). The figure shows that the mean upward motion over the warm pool is about one order magnitude larger than the mean downward motion over the cold pool. Figure 2 also shows a

weak upward motion near 200 mb over the cold pool due to the existence of ice clouds as discussed below. The vertical motion over the warm pool is maintained by latent heat released by deep convection as revealed by the mean rainfall over the warm pool shown in Fig. 1. On the other hand, rainfall is absent over the cold pool due to the existence of downward motion. The temperature distribution (not shown) show that the largest difference in lapse rates between warm pool and cold pool is in the lower troposphere where the cold pool is stable while the warm pool is unstable. The stability effectively prevents the development of convection in the cold pool.

The model heat and moisture budgets are shown in Fig. 3. The heat budget in the warm pool (Fig. 3a) shows the well known fact that condensation heating and advective cooling are dominant in the heat budget. However, because the two almost cancel each other, their residual is in near balance with radiation. The radiative heating (cooling) in the middle (upper) troposphere reflects the effect of high clouds. In contrast to the warm pool budget, the heat budget in the cold pool (Fig. 3b) is balanced between radiative cooling and advective warming in the whole troposphere except near 200 mb where the two terms reverse signs due to the presence of ice clouds. The presence of ice clouds also contributes to evaporative cooling near 500 mb as discussed below. The heat budget indicates that while deep convection is a dominant process in the warm pool, radiative process is crucial in maintaining the heat balance in the cold pool. Because the heat balance determines the subsidence in the cold pool that in turn affects the ascending motion in the warm pool, the radiative cooling plays an important role in maintaining the equilibrium.

Sources of water vapor over the cold pool include evaporation from the sea surface, and of clouds advected from the surrounding regions. In the current experiment (R1), the moisture

budget in the cold pool is shown in Fig. 3c. The figure shows a moistening peak near 250-400 mb by advection, a moistening peak by evaporation near 550 mb, and a drying peak near 200 mb by condensation. These peaks are balanced by vertical eddy flux convergence. The most likely explanation for these sources and sinks is that water vapor being advected from the warm pool to the cold pool in the upper troposphere (above 450 mb) where they form ice clouds and being maintained by unstable temperature stratification due to cloud-radiative effect. The precipitation in ice clouds (snow and graupel) falls and evaporates near 550 mb. The above explanation is supported by the fields of cloud, water vapor anomalies, and zonal wind at day 40 shown in Fig. 4. These figures show the existence of deep convection over the warm pool in the central domain (Fig. 4a) that is associated with extensive upper-level moisture anomalies (Fig. 4b) due to the upper-level divergent and low-level convergent circulation (Fig. 4c). The upper-level moisture is the source for ice clouds extending outward from warm pool to cold pool where the ice clouds disappeared around 550 mb. This is the same level where evaporation appears in the water vapor budget (Fig. 3c). The spatial structure of upper-level ice clouds, water vapor, and zonal wind winds above 300 mb over the cold pool shows the existence of convective updrafts and downdrafts, indicating a strong radiative-convective interaction. This is consistent with the radiative heating distribution in the upper troposphere in Fig. 3b.

4. PERTURBED EQUILIBRIUM SOLUTION

We now examine the change of equilibrium solution to perturbed SST contrast in experiment R, R1, and R2 that are specified at 2.5°C, 3.5°C and 4.5°C, respectively. We first show in Fig. 5a the difference of ensemble mean temperature, specific humidity, and vertical velocity in the two regimes between R1 and R. The results indicate that the mean vertical motion becomes more upward (downward) in the warm (cold) pool as the SST gradient increases

from 2.5°C to 3.5°C. This leads to a more humid atmosphere in the warm pool and a drier atmosphere (except the boundary layer and upper troposphere near 300 mb) in the cold pool. Figure 5a further shows that equilibrium air temperature in both regimes becomes warmer. The warming is a result of destabilization (stabilization) over the warm (cold) pool by enhanced upward (downward) motion that leads to more condensational heating over the warm pool and more subsidence warming and less condensational heating over the cold pool (Fig. 6a). Note that that the change in radiative heating over the cold pool is small.

As the SST gradient increases from 3.5°C to 4.5°C from R1 and R2, the mean vertical motion remains almost unchanged while the temperature and humidity changes similarly as those from R to R1 except with weaker amplitudes (Fig. 5b). The nearly identical vertical motion between R2 and R1 can be explained by the difference heat budgets in the cold pool region for R1-R and R2-R1 shown in Fig. 6. The figure shows that radiative cooling in the cold pool between R and R1, and between R2 and R1 are quite small, indicating it remains almost the same in all three experiments. As a result, the difference heat budget for R1-R is balanced between a reduced condensation heating and increased subsidence warming. In fact, the existence of latent heating in the cold pool only occurs in the Experiment R as SST gradient is weak (2.5°C), not in the Experiment R1 and R2 due to the expansion of subsidence over the entire cold pool (figure not shown). Thus subsidence warming do not change significantly from R1 to R2 because of the absence of latent heating and the insensitivity of radiative cooling in the three experiments. In the absence of clouds in the cold pool, therefore, radiative cooling effectively regulates subsidence motion that in turn determines the ascending motion in the warm pool in the current experiments.

5. WATER VAPOR AND CLOUD FEEDBACKS TO SST CHANGES

In this section, we investigate the effect of water vapor and clouds on energy flux at top of the atmosphere (TOA) and surface corresponding to SST changes. First, we examine the time and domain averaged energy fluxes at TOA, N_{TOA}, and surface, N_{SFC}, and the energy transport out of the tropics, F_{AH}, as defined by

$$N_{TOA} = SW - LW, \tag{2}$$

$$N_{SFC} = SW - LW - H_E - H_S, \tag{3}$$

$$F_{AH} = N_{SFC} - N_{TOA} \tag{4}$$

In the above expressions, SW and LW denote net downward shortwave and net upward longwave radiation, H_E and H_S denote latent heat and sensible heat fluxes. The time and domain averaged N_{TOA}, N_{SFC}, and F_{AH} of the model tropical climate from Experiment R is 92 Wm^{-2}, 33.9 Wm^{-2}, and -58.1 Wm^{-2}, respectively as shown in Table 2. These averaged energy are comparable to current tropical climate values.

Table 2 Time and domain averaged energy fluxes at TOA and surface (Wm^{-2})

	N_{TOA}	N_{SFC}	F_{AH}
R	92.0	33.9	-58.1
R1–R	4.5	-8.2	-12.7
R2–R1	-0.6	-13.5	-12.9
W–R	2.9	-5.1	-8.0

Table 2 also shows the differences of N_{TOA}, N_{SFC}, and F_{AH} between different experiments. First we note that the difference of energy transport out of the tropics (ΔF_{AH}) corresponding to R1-R and R2-R1 are larger compared with that for W-R. Because the domain-mean circulation

and incoming solar radiation are kept the same in all experiments, ΔF_{AH} are resulted mostly from enhanced latent heat fluxes over the warm pool due to increased SST gradient between warm pool and cold pool. Next we note that changes of the surface energy balances ΔN_{SFC} is generally larger than ΔN_{TOA}. However, since ΔN_{SFC} is largely affected by the prescribed SST, whereas ΔN_{TOA} is found to be dominated by the changes in LW due to water vapor and cloud greenhouse effects. We shall focus on the water vapor and cloud feedbacks below based on the change of energy flux at TOA.

To discuss the change of net energy flux at TOA between different experiments, ΔN_{TOA} can be expressed by

$$\Delta N_{TOA} = \Delta SW - \Delta LW = \Delta SW - \Delta(\sigma T^4) + \Delta G_{clear} + \Delta c_{LW} \quad (5)$$

where $G_{clear} = \sigma T^4 - LW_{clear}$ denotes atmospheric greenhouse effect, and $c_{LW} = LW_{clear} - LW$ is defined as longwave cloud forcing. Note that $G_{clear} + c_{LW} = \sigma T^4 - LW$ is the total greenhouse effect by water vapor and cloud. The energy fluxes at TOA for Experiment R and the differences from other experiments are listed in Table 3. Subject to an increased surface emission, $\Delta(\sigma T^4)$ from R to R1 (1.9 Wm^{-2}), R1 to R2 (2 Wm^{-2}), and R to W (6.2 Wm^{-2}), the corresponding values of ΔSW averaged over the whole domain are smaller than the values of ΔLW (Table 3). Note that the values of ΔSW averaged over the warm pool and cold pool separately are actually quite large but of opposite signs (Table 4). From R to W, SST is uniformly higher by 1°C, and both G_{clear} and c_{LW} increase by about 5 Wm^{-2}, indicating an equally important greenhouse warming by water vapor and clouds. On the other hand, negative values of ΔG_{clear} corresponding to R1-R and R2-R1 reveal a strong cooling by outgoing LW_{clear} at TOA (not shown) due to the change in water vapor distribution as shown in Fig. 5. These negative water vapor greenhouse effect are all weaker than the greenhouse warming by clouds as shown by ΔC_{LW} in Table 3. Table 3 further

shows that, in terms of the ratio between total greenhouse effect and surface emission, $(\Delta G_{clear}+\Delta c_{LW})/\Delta(\sigma T^4)$, total greenhouse effect increases more efficiently from R to R1 (5.7 Wm^{-2} vs. 1.9 Wm^{-2}) than from R1 to R2 (0.8 Wm^{-2} vs. 2.0 Wm^{-2}). Similarly, the change from R to R1 is more efficient than the change from R to W (9.8 Wm^{-2} vs. 6.2 Wm^{-2}). But the change from R1 to R2 is less efficient than the change from R to W. This indicates that the change of water vapor and cloud greenhouse effects to surface warming varies significantly with internal dynamic response which is regulated by the radiative cooling in the cloud-free subsidence regime.

Table 3 Energy fluxes at TOA and greenhouse effect averaged over the whole domain (Wm^{-2})

Exp.	SW	LW	LW_{clear}	σT^4	G_{clear}	C_{LW}
R	303.6	211.6	302.9	458.9	156.0	91.3
R1–R	0.7	-3.8	4.1	1.9	-2.2	7.9
R2–R1	0.7	1.2	2.7	2.0	-0.7	1.5
W–R	-0.7	-3.6	1.4	6.2	4.8	5.0

Table 4 Energy fluxes at TOA averaged over the warm pool and cold pool (Wm^{-2})

	Warm Pool		Cold Pool	
	SW	LW	SW	LW
R	238.5	155.5	333.2	237.1
R1–R	-14.6	-1.7	7.6	-4.7
R2–R1	5.9	4.4	-1.6	-0.2
W–R	-11.1	-1.3	4.0	-4.6

Clouds play an important role in the above results. Table 5 shows fractional areas of raining clouds of convective type (A_{CR}) and stratiform type (A_{SR}), and of non-raining clouds (A_{NR}) over warm pool and cold pool for different experiments (see Sui et al. 1994 for definition of various cloud type in the model). From R to R1, active clouds (A_{CR} and A_{SR}) increase by 5.6% and passive clouds (A_{NR}) decrease by 1.9% over the warm pool. The opposite occurs over the cold pool where A_{CR} and A_{SR} decrease by 3.8 % and A_{NR} increases by 6.5 %. This is a response to the increasing strength of circulation as discussed in the previous section (Fig. 5). Associated with these cloud changes from R to R1, the LW over the cold pool decreases by 4.7 Wm^{-2} (Table 4), likely due to the increased optically thin cirrus cloud (ΔA_{NR}=6.5%) and the upper tropospheric humidity (see Fig. 5). On the other hand, the SW heating increases by 7.6 Wm^{-2}, due to the reduced amount of raining clouds ($\Delta A_{CR}+\Delta A_{SR}$= -3.8 %) with high reflective. Over the warm pool, SW heating decreases by 14.6 Wm^{-2}, and the LW cooling decreases by 1.7 Wm^{-2} from R to R1. This is related to the net increase of optically thick clouds ($\Delta A_{CR}+\Delta A_{SR}$=5.6%). A similar change in clouds and radiative fluxes are also found from R to W except that cirrus clouds over the warm pool also increase (ΔA_{NR}= 2.4 %). From R1 to R2, cloud amount does not change significantly over the cold pool, so is the corresponding change of radiative fluxes at TOA. Over the warm pool, all three types of clouds decrease from R1 to R2. This causes an increase in both SW heating and LW cooling.

Table 5 Fractional area of clouds (%)

	Warm Pool		Cold Pool	
	$A_{CR}+A_{SR}$	A_{NR}	$A_{CR}+A_{SR}$	A_{NR}
R	32.6	61.3	4.1	43.7
R1–R	5.6	-1.9	-3.8	6.5
R2–R1	-1.1	-1.1	0.1	0.8
W–R	1.7	2.4	-2.7	6.4

6. CONCLUSION AND DISCUSSION

In this study, we investigate the equilibrium states of the tropical atmosphere in different surface forcing conditions using a 2D version of the Goddard Cumulus Ensemble (GCE) Model. We perform experiments by integrating the model over an ocean domain of 5120 km with an imposed mean vertical motion and idealized SST distributions of a warm pool about 1588 km wide in the center and a cold pool in the rest of the domain. Experiments are carried out by varying imposed SST in warm pool and/or in cold pool. For each experiment, the model is integrated for 50-70 days to reach equilibrium. A mean ascending motion over the warm pool and a descending motion over the cold pool are developed in each of the simulations. As a result, the ascending branch of the tropical atmosphere is humid and the descending atmosphere is dry.

In the experiment R, R1, and R2, the warm pool SST are specified at 28.5°C, 29.5°C, and 30.5°C, respectively while the cold pool SST is specified at 26°C. The most notable difference among the three experiments is the strength of equilibrium circulation that increases appreciably as the warm pool SST changes from 28.5°C to 29.5°C, but remains almost unchanged as SST changes from 29.5°C to 30.5°C. The equilibrium temperature in each experiment is related to the imposed sea surface temperature such that a warmer SST in the warm pool leads to warmer temperature over the warm pool as well as over the cold pool. But the humidity is highly dependent on the circulation such that the stronger ascending atmosphere over the warm pool is more humid while the stronger descending atmosphere over the cold pool is drier.

The differences of equilibrium circulation among R, R1 and R2 is determined by the heat budget in the cold pool that is primarily balanced between radiative cooling and advective warming. The subsidence in the cold pool in turn affects the ascending motion in the warm pool. Since radiative cooling in the subsidence regime changes little in all three experiments due to the

slow varying clear sky outgoing longwave radiation with humidity, an enhanced subsidence warming over the cold pool from R to R1 is resulted from increased subsidence area. From R1 to R2, subsidence area further expands into the warm pool region when the warm pool SST exceeds 29.5°C. As a result, subsidence warming is capped by radiative cooling.

The above results indicate that radiative cooling in the cold pool acts as an effective regulator on the development of clouds and water vapor as is evident in the water vapor and cloud feedbacks to the SST perturbations. This is revealed in the change of energy at the top of the atmosphere (TOA) in the experiments. The TOA energy is generally dominated by the change in longwave radiation while the change in shortwave radiation is largely canceled between the warm pool and cold pool. The change of longwave radiation at TOA is largely affected by cloud and water vapor greenhouse effect (c_{LW} and G_{clear}) that is sensitive to the change of δSST. For δSST<3.5°C, Δc_{LW} is about 8 Wm^{-2} and ΔG_{clear} is about -2 Wm^{-2} per degree change of δSST. The large value of Δc_{LW} is associated with increased total clouds in response to enhanced mean upward motion over the warm pool due to more developing clouds (rain-producing) than dissipating clouds and the reversed situation over the cold pool. For δSST>3.5°C, clouds over the warm pool decrease with increasing SST, and the change in c_{LW} is much smaller and near cancel the effect of G_{clear}. In the case of uniform warming so δSST=0, the model shows that Δc_{LW} and ΔG_{clear} per degree change of SST is about the same, ~ 5 Wm^{-2}.

Note that the above estimate only holds under the imposed constraints like the imposed mean vertical motion. The result is also affected by limited domain size and idealized SST distribution. One such consequence is the model warm pool is near 100% cloudy. As a result, the model atmosphere over the warm pool is closer to the disturbed state of tropical atmosphere over the warm pool. However, the regulation effect of radiative cooling on water vapor- and cloud-

radiative forcing provides a useful reference for assessing tropical climate changes in nature or climate models.

Figure caption

Fig. 1 Time series of vertically averaged temperature (a) and moisture (b), and surface rainfall rate (c) over the warm pool (solid curves) and cold pool (dashed curves) from R1.

Fig. 2 Time mean vertical profiles of vertical velocity during the period of Day 40 to 50 over the warm pool (thick solid), cold pool (dashed), and the whole domain (thin solid) from R1. Unit is cm s^{-1}.

Fig. 3 Time-mean heat budgets averaged over the warm pool (a) and over the cold pool (b) and the time mean moisture budget over the cold pool (c) from R1. Note that the scale of condensation heating and vertical advection are 10 times larger than the other two terms in (a)

Fig. 4 Snap shot of (a) total cloud content, q_c, (b) perturbation water vapor mixing ratio, q_v', and (c) zonal wind, u at Day 40 from R1. In the above figures, areas of $q_c > 10^{-3}$ g kg^{-1} and positive q_v' and u are shaded. Contour interval of q_c q_v', and u are, respectively, 0.02 g kg^{-1} starting at 0.01 g kg^{-1}, 2 g kg^{-1} starting at ±1 g kg^{-1}, and 2 m s^{-1}.

Fig. 5 Vertical profiles of difference of c_pT, Lq_v, and w between R1-R (upper) and R2-R1 (lower) averaged over the warm pool and cold pool. Units of c_pT and Lq_v are Jg^{-1}, w is cm s^{-1}.

Fig. 6 Vertical profiles of difference of heat budget between R1-R (upper) and R2-R1 (lower).

REFERENCES

Gadgil, S., P. V. Joseph, and N. V, Joshi, 1984: Ocean-atmospheric coupling over monsoon regions. *Nature*, **312**, 141-143.

Graham, N., and T. P. Barnett, 1987: Sea surface temperature, surface wind divergence, and convection over tropical oceans. *Science*, **238**, 657-659.

Held, I. M., R. S. Hemler, and V. Ramaswamy, 1993: Radiative-convective equilibrium with explicit two-dimensional moist convection. *J. Atmos. Sci.*, **23**, 3909-3927.

Lau, K.-M., C.-H. Sui and W.-K. Tao, 1993: A preliminary study of the tropical water cycle using the Goddard Cumulus Ensemble model. *Bull. Amer. Meteor. Soc.* **74**, 1313-1321.

Lau, K.-M., C.-H. Sui, M.-D. Chou and W.-K. Tao, 1994: Cirrus cloud thermostat effect for tropical sea surface temperature-fact or fiction. *Geophysical Research Letter* , **21**, 1157-1160, 1994.

Lau, K.-M, H.-T. Wu, S. Bony, 1997: The role of large-scale atmospheric circulation in the relationship between tropical convection and sea surface temperature. J. Climate, 10, 381-392..

Li, X., C.-H. Sui, K.-M. Lau, and M.-D. Chou, 1999: Large-scale forcing and cloud-radiation interaction in the tropical deep convective regime. *J. Atmos. Sci.* **56**, 3028-3042.

Lindzen, R. S., 1990: Some coolness concerning global warming. *Bull. Amer. Meteor. Soc.*, **71**, 288-299.

Pierrehumbert, R. T., 1995: Thermostats, radiator fins, and the local runaway greenhouse. *J. Atmos. Sci.* **52**, 1784-1806.

Sui, C.-H., K.-M. Lau, and A. K. Betts, 1991: An equilibrium model for the coupled ocean-atmosphere boundary layer in the tropics. *J. Geophys. Res.* **96**, 3151-3163.

Sui, C.-H., K.-M. Lau, W.-K. Tao, M. D. Chou, and J. Simpson, 1993: Simulated water and radiation budgets in the tropics. Proc. 20th Conf. On Hurricanes and Tropical Meteorology, **51**, 291-294.

Sui, C.-H., K.-M. Lau, W.-K. Tao and J. Simpson, 1994: The tropical water and energy cycles in a cumulus ensemble model. Part 1: Equilibrium climate. *J. Atmos. Sci.* **51**, 711-728, 1994.

Sui, C.-H., X. Li, and K.-M. Lau, 1998: Radiative-convective processes in simulated diurnal variations of tropical oceanic convection. *J. Atmos. Sci.*. **55**, 2345-2357.

Sun, D. Z., and R. S. Lindzen, 1993: On the distribution of tropical tropospheric water vapor.

Tao, W.-K., and J. Simpson, 1993: The Goddard Cumulus Ensemble Model. Part 1: Model description. *Terrestrial, Atmospheric and Oceanic Science*, **4**, 35-72.

Tao, W.-K., J. Simpson, C.-H. Sui, C.-L. Shie, B. Zhou, K.-M. Lau, and M. Moncrieff, 1999: On equilibrium states simulated by cloud-resolving models. *J. Atmos. Sci.* **56**, 3128-3139.

Tompkins, A. M. and G. C. Craig, 1998: Radiative-convective equilibrium in a three-dimensional cloud ensemble model. *Q. J. R. Meteorol. Soc.*, **124**, 2073-2098.

Waliser, D. E., 1996: Formation and limiting mechanisms for very high sea surface temperature: Linking the dynamics and thermodyanmics. *J. Climate*, **9**, 161-188.

Wu, X., and M. W. Moncrieff, 1998: Effects of sea surface temperature and large-scale dynamics on the thermodyanmics equilibrium state and convection over the tropical western Pacific.

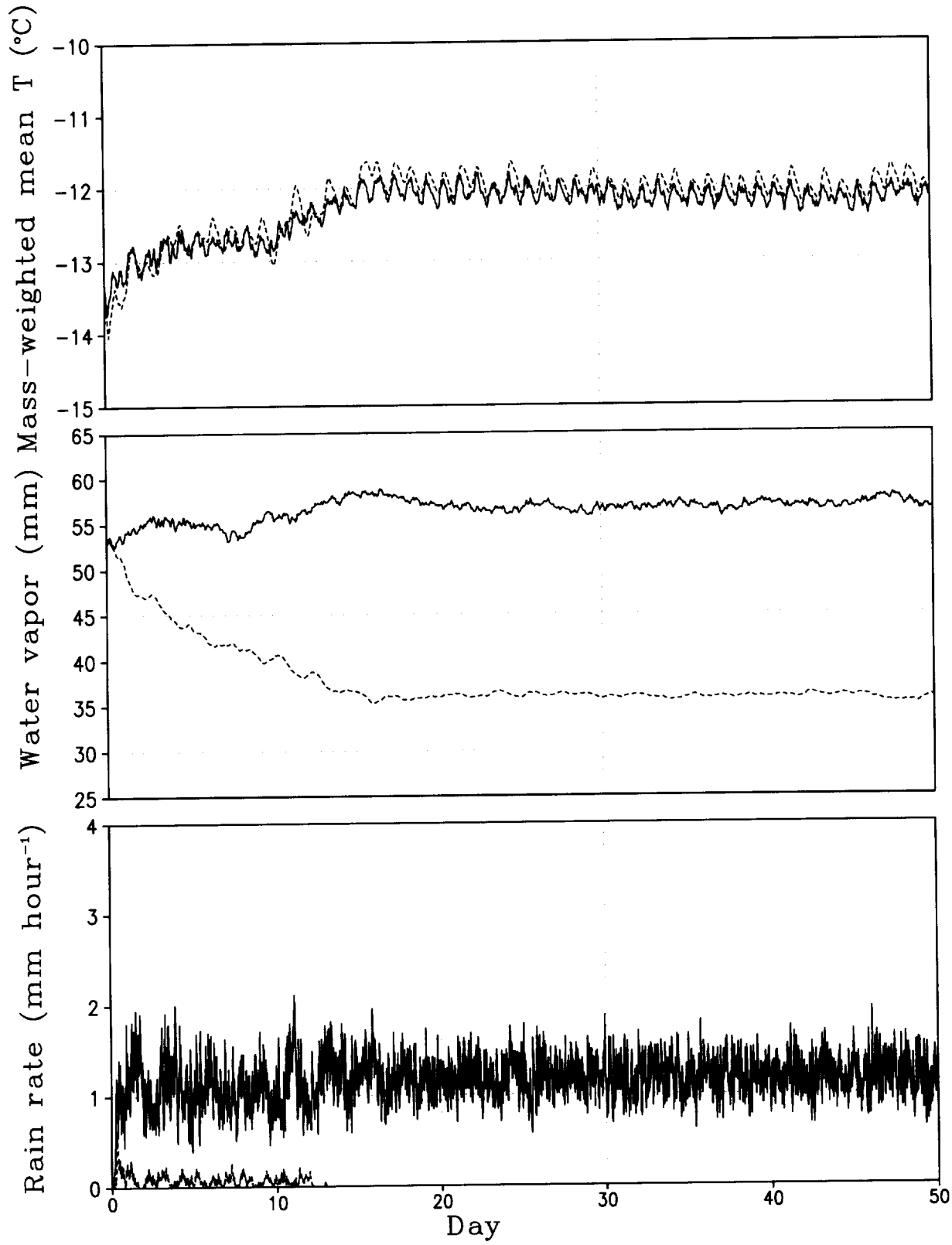
Mass-weighted mean T (°C)
-10
-11
-12
-13
-14
-15
Water vapor (mm)
65
60
55
50
45
40
35
30
25
Rain rate (mm hour⁻¹)
4
3
2
1
0
0
10
20
30
40
50
Day

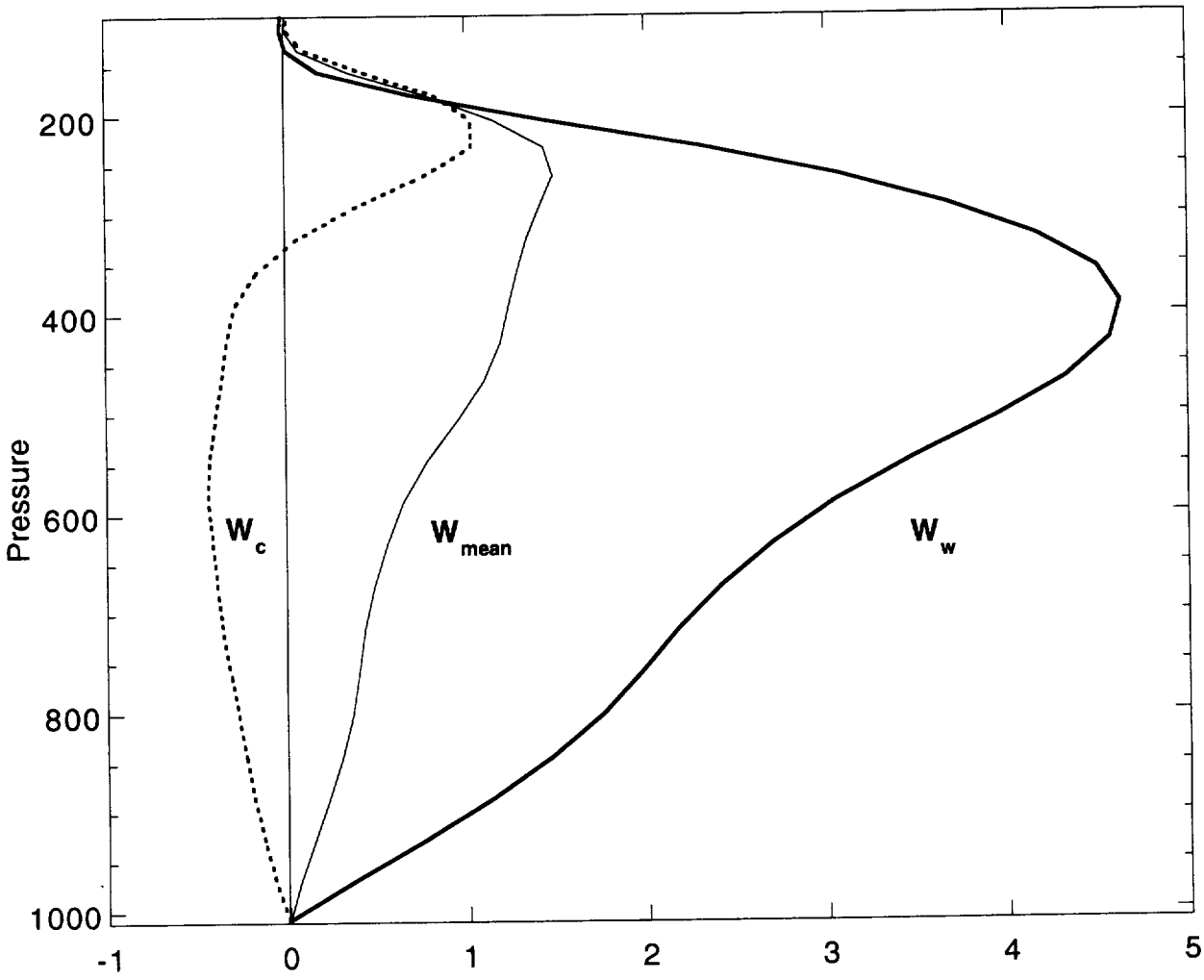
Pressure
200
400
600
800
1000
-1
0
1
2
3
4
5
W_c
W_mean
W_w

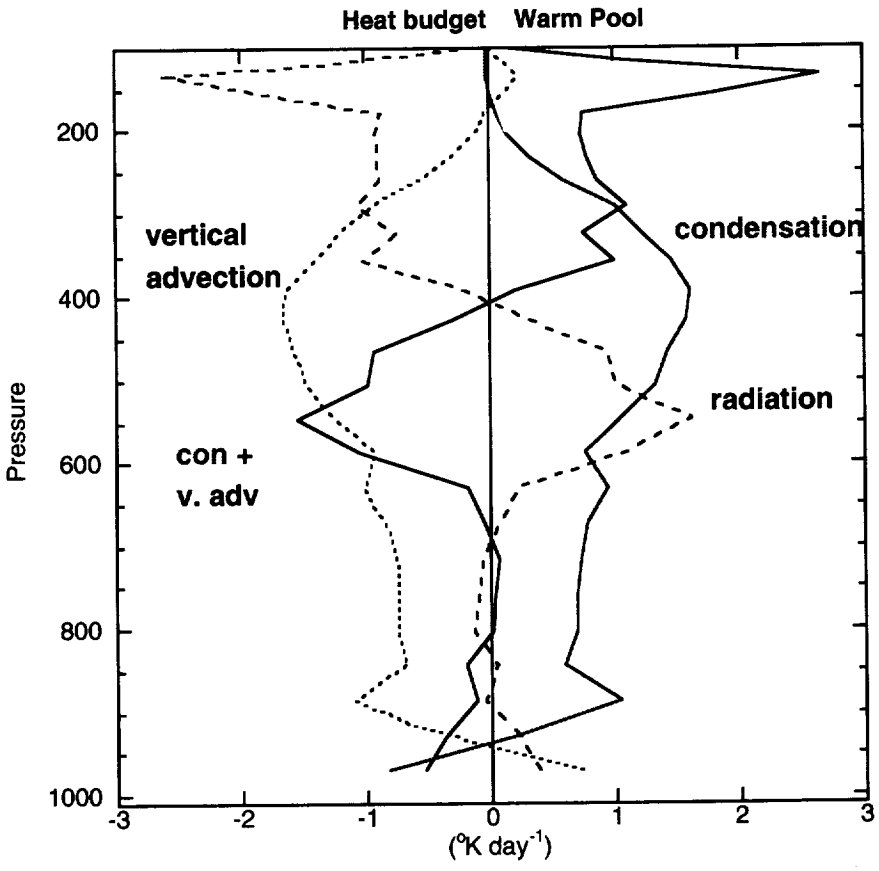
Heat budget Warm Pool
Pressure
200
400
600
800
1000
-3
-2
-1
0
1
2
3
(°K day-1)
vertical
advection
condensation
radiation
con +
v. adv

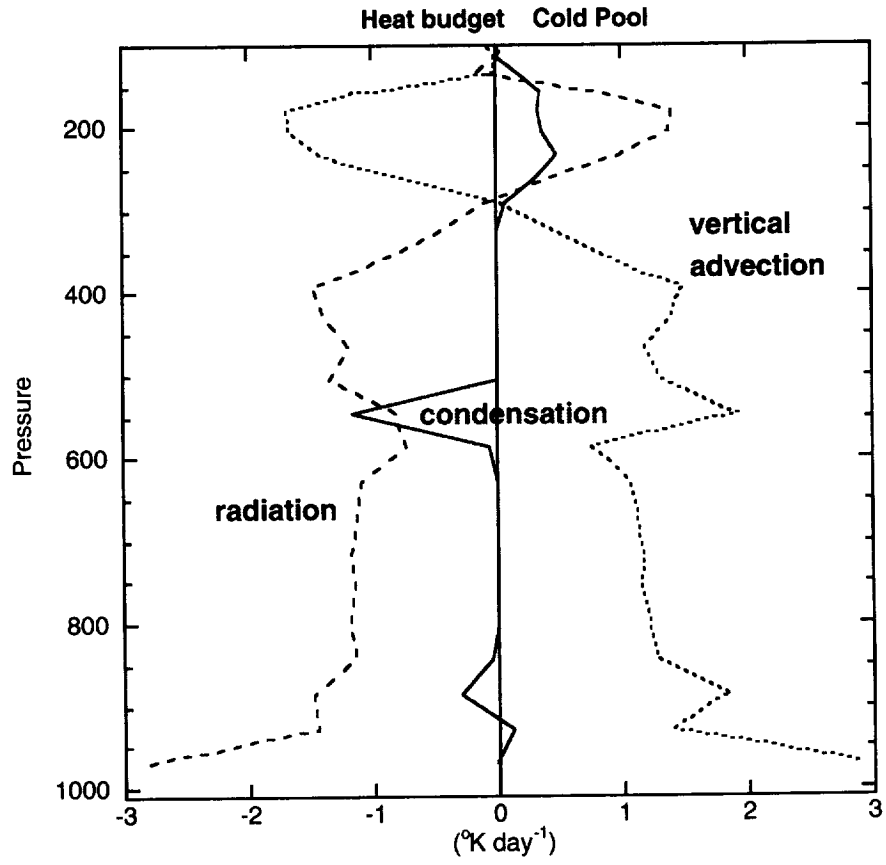
Heat budget Cold Pool
Pressure
200
400
600
800
1000
-3
-2
-1
0
1
2
3
(°K day-1)
vertical
advection
condensation
radiation

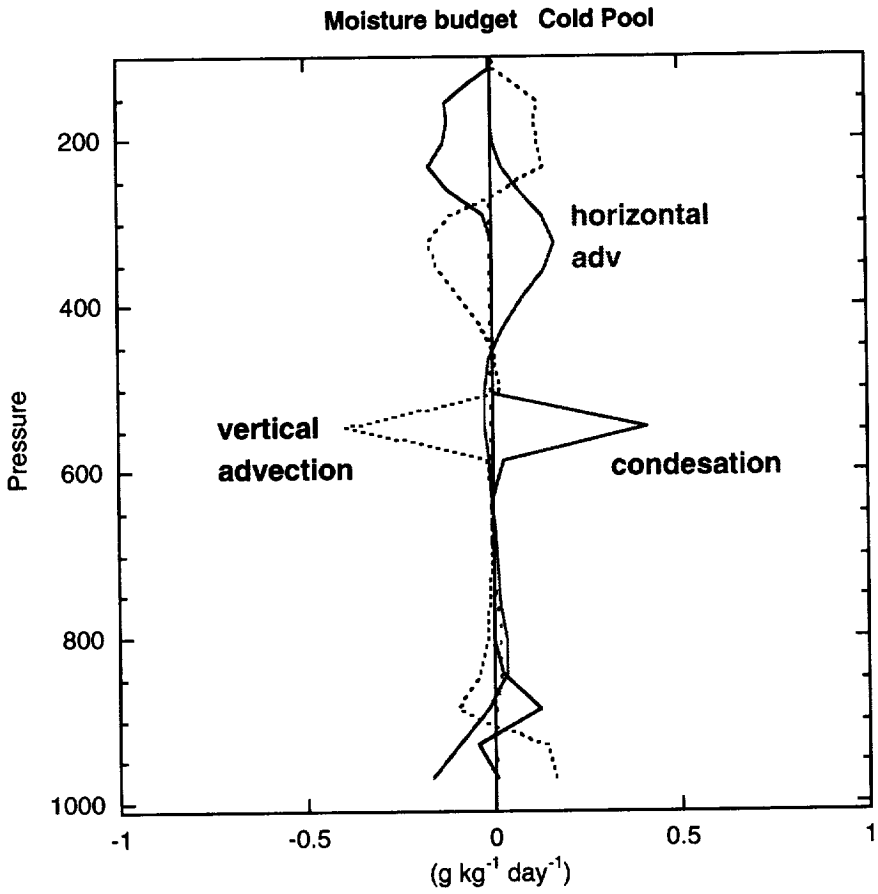
Moisture budget Cold Pool
Pressure
200
400
600
800
1000
-1
-0.5
0
0.5
1
(g kg-1 day-1)
horizontal
adv
vertical
advection
condesation

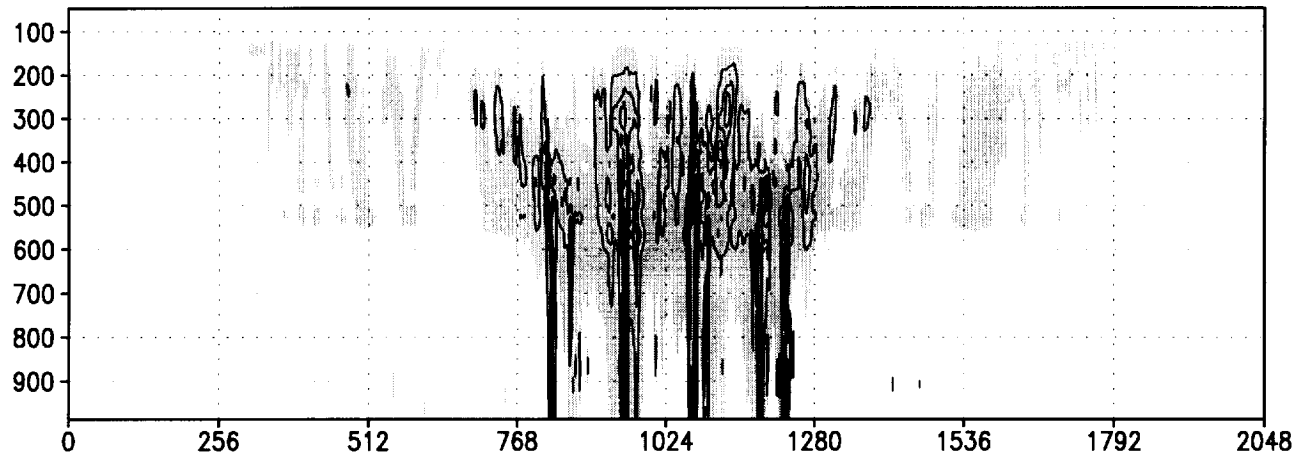
100
200
300
400
500
600
700
800
900
0
256
512
768
1024
1280
1536
1792
2048

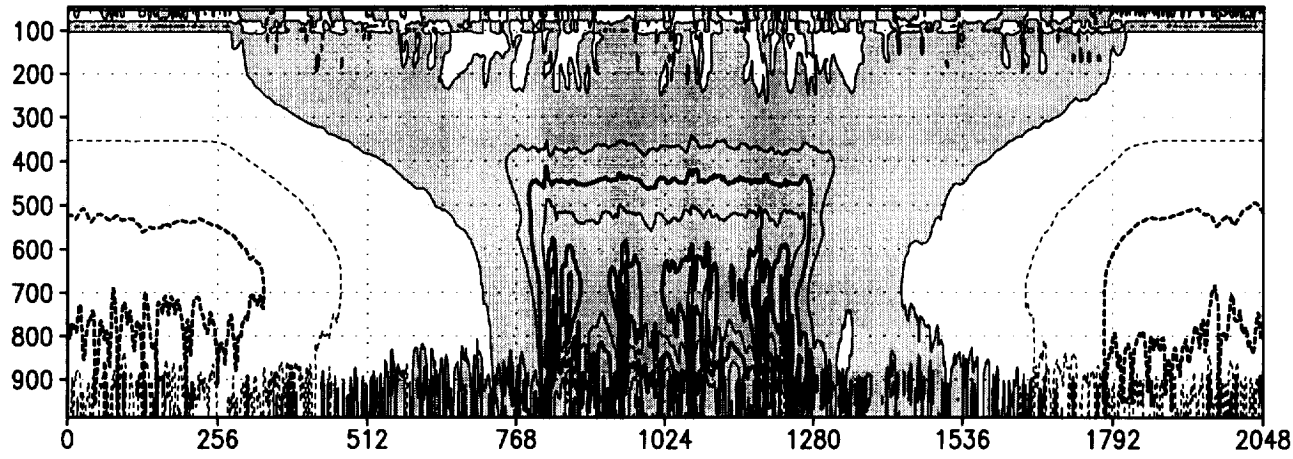
100
200
300
400
500
600
700
800
900
0
256
512
768
1024
1280
1536
1792
2048

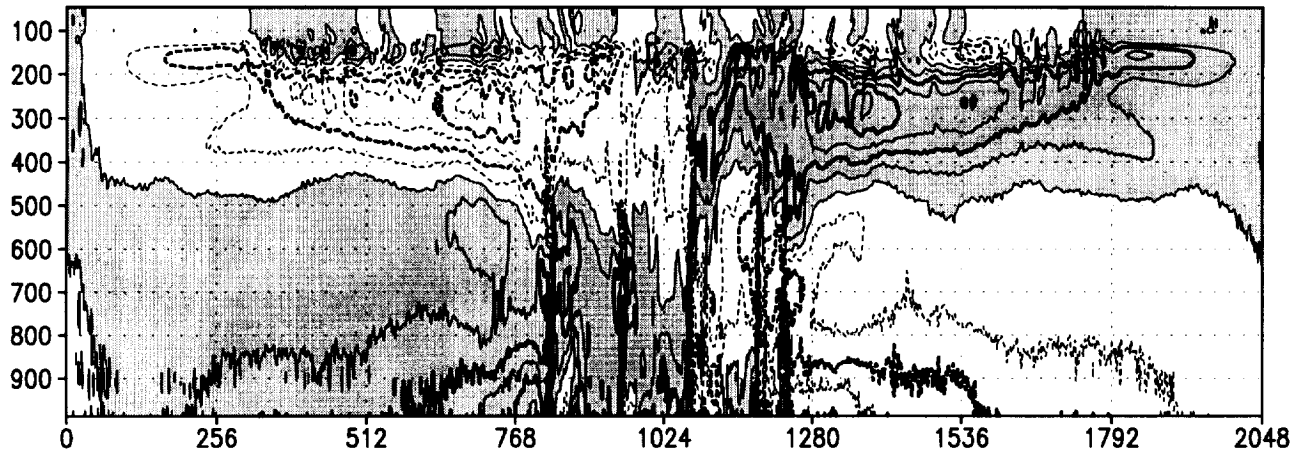
100
200
300
400
500
600
700
800
900
0
256
512
768
1024
1280
1536
1792
2048

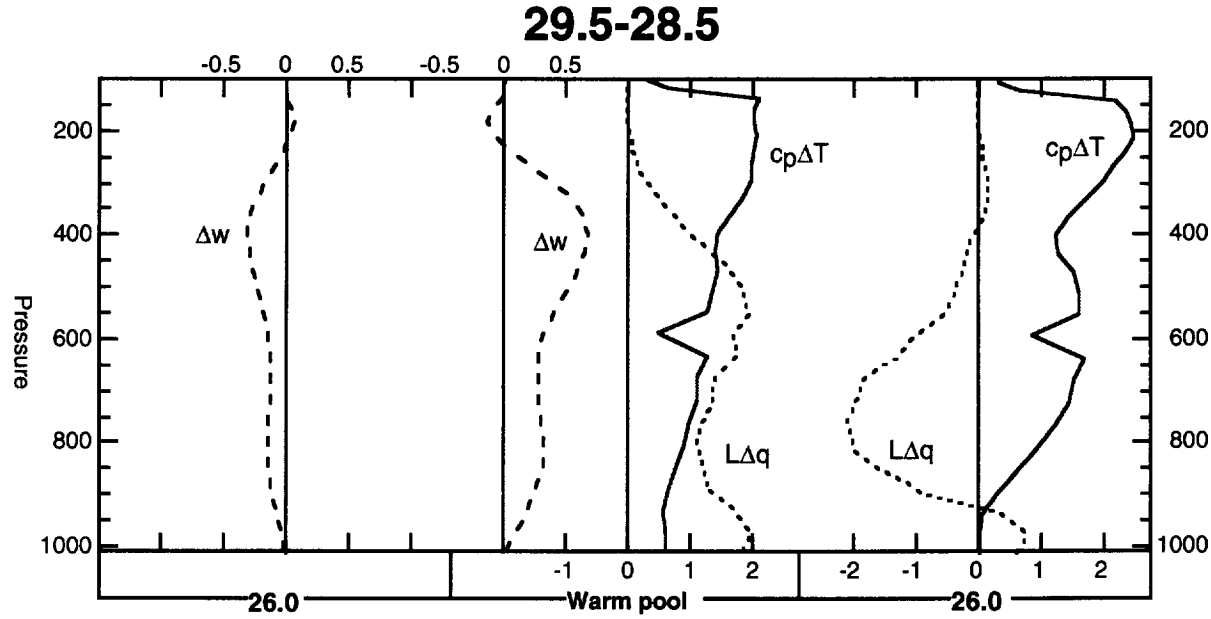
29.5-28.5
-0.5 0 0.5 -0.5 0 0.5
200
400
600
800
1000
Pressure
Δw
Δw
cpΔT
LΔq
cpΔT
LΔq
-1 0 1 2
-2 -1 0 1 2
26.0
Warm pool
26.0

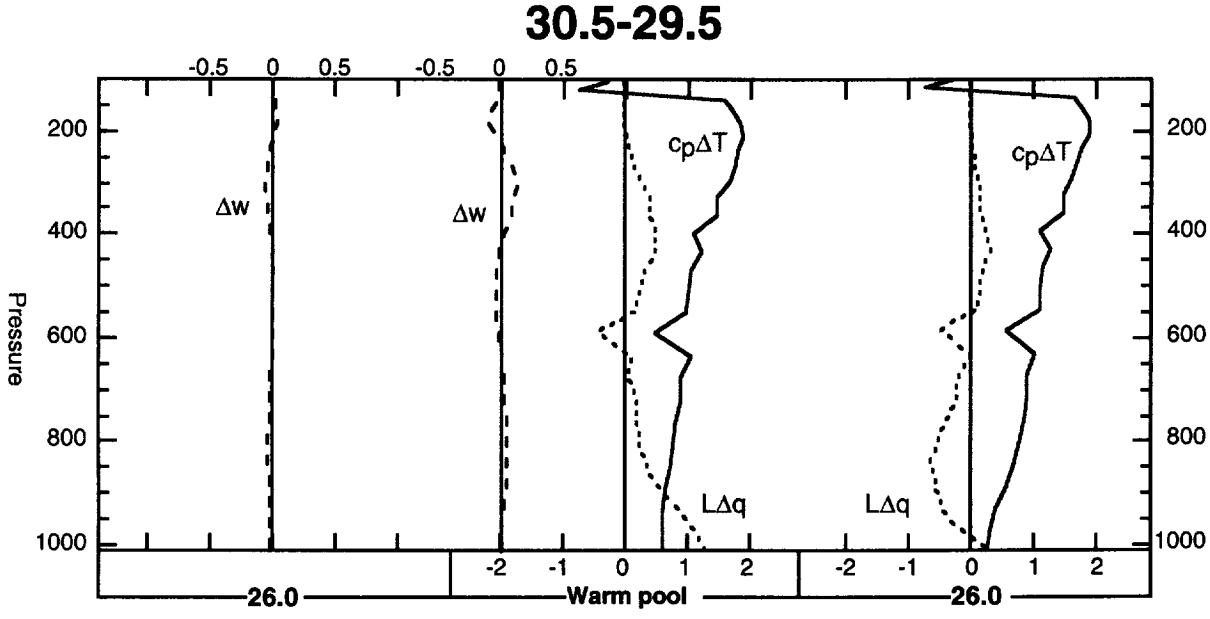
30.5-29.5
-0.5 0 0.5 -0.5 0 0.5
200
400
600
800
1000
Pressure
Δw
Δw
cpΔT
LΔq
cpΔT
LΔq
-2 -1 0 1 2
-2 -1 0 1 2
26.0
Warm pool
26.0

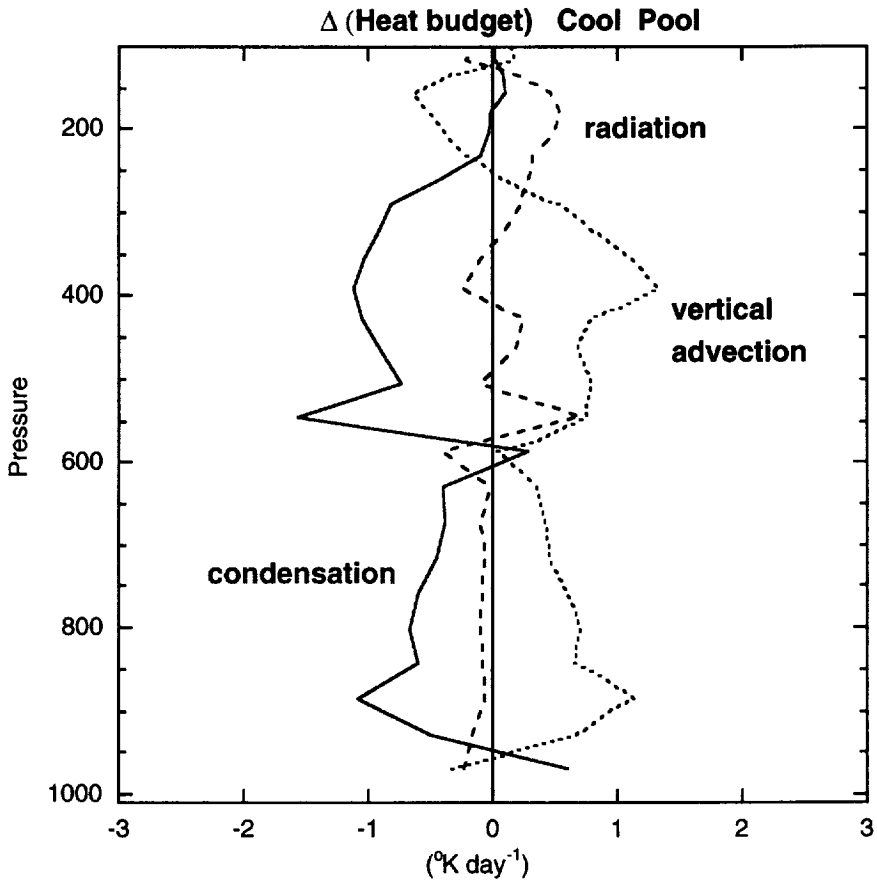
Δ (Heat budget) Cool Pool
radiation
vertical
advection
condensation
Pressure
200
400
600
800
1000
-3
-2
-1
0
1
2
3
(°K day-1)

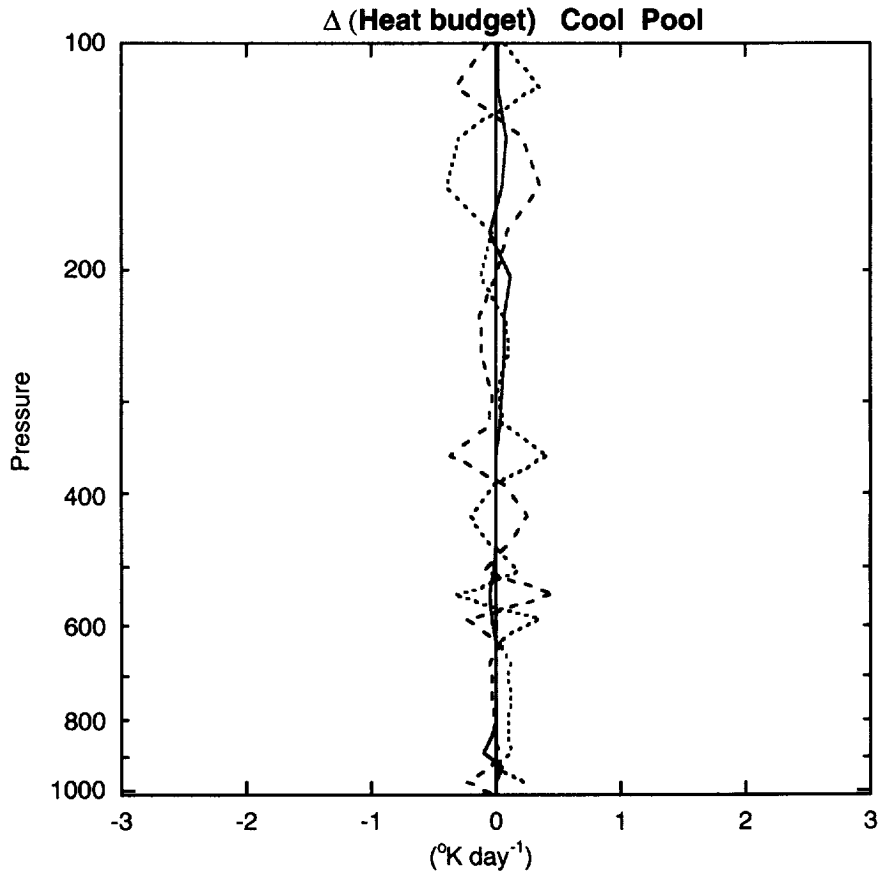
Δ (Heat budget) Cool Pool
Pressure
100
200
400
600
800
1000
-3
-2
-1
0
1
2
3
(°K day-1)